


RESEARCH ARTICLE

Lipopolysaccharide-induced alteration of mitochondrial morphology induces a metabolic shift in microglia modulating the inflammatory response in vitro and in vivo

Syam Nair^{1,2}  | Kristina S. Sobotka^{1,2} | Pooja Joshi³ | Pierre Gressens^{3,4} | Bobbi Fleiss^{3,4,5} | Claire Thornton⁴ | Carina Mallard^{1,2} | Henrik Hagberg^{1,4,6}

¹Centre of Perinatal Medicine and Health, The Sahlgrenska Academy, University of Gothenburg, Gothenburg, Sweden

²Institute of Neuroscience and Physiology, The Sahlgrenska Academy, University of Gothenburg, Gothenburg, Sweden

³PROTECT, INSERM, Université Paris Diderot, Paris, France

⁴Centre for the Developing Brain, Department of Division of Imaging Sciences and Biomedical Engineering, King's College London, King's Health Partners, St. Thomas' Hospital, London, United Kingdom

⁵School of Health and Biomedical Sciences, RMIT University, Bundoora, Victoria, Australia

⁶Institute of Clinical Sciences, The Sahlgrenska Academy, University of Gothenburg, Gothenburg, Sweden

Correspondence

Henrik Hagberg, Department of Obstetrics and Gynecology, Institute of Clinical Sciences, Journalvägen 6, 41685 Gothenburg, Sweden.
Email: henrik.hagberg@gu.se

Funding information

Biomedical Research Centre Award to Guy's & St Thomas' NHS Foundation Trust in partnership with King's College London and King's College Hospital NHS Foundation Trust; Ahlen Foundation; ALF-GBG, Grant/Award Numbers: 426401, HH; 432291, CM, 432291, 426401; ERA-NET, Grant/Award Numbers: EU; VR 529-2014-7, VR 529-2014-7551; Hjärfonden; Swedish Medical Research Council, Grant/Award Numbers: VR 2015-02493, VR 2012-2992; Torsten Söderbergs Stiftelse, Grant/Award Number: M98/15, CM; Wellcome Trust, Grant/Award Number: WT094823; King's College Hospital NHS Foundation Trust; King's College London; National Institute for Health Research; Frimurare Barnhusdirektionen; Torsten Söderberg, Grant/Award Number: M98/15; Leducq Foundation, Grant/Award Number: DSRRP34404; Ahlen Foundation; Brain Foundation; Medical Research Council; Wellcome Trust, Grant/Award Number: WT094823

Accumulating evidence suggests that changes in the metabolic signature of microglia underlie their response to inflammation. We sought to increase our knowledge of how pro-inflammatory stimuli induce metabolic changes. Primary microglia exposed to lipopolysaccharide (LPS)-expressed excessive fission leading to more fragmented mitochondria than tubular mitochondria. LPS-mediated Toll-like receptor 4 (TLR4) activation also resulted in metabolic reprogramming from oxidative phosphorylation to glycolysis. Blockade of mitochondrial fission by Mdivi-1, a putative mitochondrial division inhibitor led to the reversal of the metabolic shift. Mdivi-1 treatment also normalized the changes caused by LPS exposure, namely an increase in mitochondrial reactive oxygen species production and mitochondrial membrane potential as well as accumulation of key metabolic intermediate of TCA cycle succinate. Moreover, Mdivi-1 treatment substantially reduced LPS induced cytokine and chemokine production. Finally, we showed that Mdivi-1 treatment attenuated expression of genes related to cytotoxic, repair, and immunomodulatory microglia phenotypes in an in vivo neuroinflammation paradigm. Collectively, our data show that the activation of microglia to a classically pro-inflammatory state is associated with a switch to glycolysis that is mediated by mitochondrial fission, a process which may be a pharmacological target for immunomodulation.

KEYWORDS

inflammation, metabolism, microglia, mitochondria, mitochondrial fission

1 | INTRODUCTION

Microglia contribute to normal brain development, homeostasis, and respond to pathological conditions by changing their phenotype from surveillance to pro-inflammatory, repair, regenerative, and immunomodulatory

states (Greter, Lelios, & Croxford, 2015; Tay, Savage, Hui, Bisht, & Tremblay, 2017). Studies of adult and neonatal injury and disease have conclusively shown that changes in the phenotype of microglia play a role in almost all forms of neuropathology (Solito & Sastre, 2012). Transcriptome analysis of microglia exposed to inflammatory stimuli revealed

transient upregulation of important and stimulus-specific metabolic pathways (Thion et al., 2018), strongly suggesting that energy metabolism is modulated during brain inflammation. Microglia activation in response to stimuli that includes pathogen associated proteins, such as lipopolysaccharide (LPS), is a metabolically energy expensive event (Moss & Bates, 2001).

Mitochondria, which play a central role in energy metabolism, are dynamic organelles that undergo biogenesis, fission, fusion, and mitophagy (autophagic degradation). The balance of these processes allows the reorganization of mitochondrial components and the elimination of damaged material, thereby maintaining a healthy mitochondrial population (Pickles, Vigie, & Youle, 2018; Wai & Langer, 2016). Recent studies have linked mitochondrial dynamics to energy demand, suggesting changes in mitochondrial architecture as a mechanism for bioenergetic adaptation to inflammation (Nasrallah & Horvath, 2014). By favoring either elongated or fragmented structures, mitochondria can regulate bioenergetic ability and thereby cell fate through metabolic programming (Buck et al., 2016). Although mitochondrial morphological changes are observed in response to alterations in oxidative metabolism (Hackenbrock, 1966), little is known of its role in microglia activation.

Microglia generate energy via both oxidative phosphorylation (OXPHOS) and glycolysis (Orihuela, McPherson, & Harry, 2016). OXPHOS occurs within the mitochondria and is more efficient for ATP synthesis in comparison to glycolysis. However, the preferential use of glycolysis over OXPHOS for ATP production enables activated microglia to produce ATP at a faster rate (Schuster, Boley, Moller, Stark, & Kaleta, 2015). Enhanced glycolysis supplies biosynthetic intermediates for cell growth and rapid production intermediates for cytokine production such as reactive oxygen species (ROS) thereby enabling effector functions (Chang et al., 2013; Everts et al., 2014). In macrophages or dendritic cells (DCs), pro-inflammatory stimuli cause them to undergo a metabolic switch from OXPHOS to glycolysis, a phenomenon similar to the Warburg effect (Kelly & O'Neill, 2015). Microglia share many functions and characteristics with macrophages (Butovsky & Weiner, 2018), but they are from a distinct non-hematopoietic lineage, and whether a similar switch from OXPHOS to glycolysis has not been explored in microglia.

We have previously found that both Toll-like receptor (TLR)-induced inflammation and mitochondrial dysfunction are involved in the development of neonatal brain injury (Hagberg, Mallard, Rousset, & Thornton, 2014; Mottahedin et al., 2017). We have also found that mitochondrial ROS production and inflammation are increased after neonatal brain injury associated with altered Krebs cycle and succinate accumulation in the mitochondria (Koning et al., 2017). Activation of microglia results in an altered Krebs cycle, as a result of metabolic switch promoting inflammatory gene expression (Gimeno-Bayon, Lopez-Lopez, Rodriguez, & Mahy, 2014; Leaw et al., 2017; Orihuela et al., 2016). Katoh et al. found that mitochondrial fission via the activation of dynamin-related protein 1 (DRP1) (by TLR4 stimulation) increases mitochondrial fission but they did not look in to metabolism or cytokine production in microglia (Katoh et al., 2017). Here, we add data on how TLR4 activation affects mitochondrial morphology, energy metabolism, ROS, and cytokine production in microglia. This knowledge is important given the many roles of microglia in mediating host-defenses and how these processes can mediate injury

to the brain when activation is aberrant and prolonged. ROS signaling has been demonstrated to result in damage to cell components; at the same time, ROS production is essential for host defenses (Zhang et al., 2012).

In this study, we investigated the link between mitochondrial architecture and metabolic reprogramming in primary microglia after induction to a prototypical pro-inflammatory activation state via LPS-mediated TLR4 activation. We also used the putative mitochondrial fission inhibitor, Mdivi-1 (Cassidy-Stone et al., 2008) to modulate mitochondrial dynamics *in vitro* and *in vivo*. We found that pro-inflammatory activation of microglia changes the mitochondrial dynamics including a metabolic switch from OXPHOS to glycolysis and that Mdivi-1 reverses these effects and the expected LPS-induced cytokine production and ROS production *in vitro*. Furthermore, we investigated the effect of Mdivi-1 in an *in vivo* paradigm of neuroinflammation and found that Mdivi-1 reduced the expression of genes related to cytotoxic, repair, and immunomodulatory microglia phenotypes.

2 | MATERIALS AND METHODS

2.1 | Animals of *in vitro* experiments

Pregnant C57BL/6 mice were sourced from Charles River Laboratories International (Sulzfeld, Germany). C57BL/6J-Tg(CAG-Cox8/EGFP)49Rin mice (Cox8/EGFP; RBRC02250) expressing endogenous green fluorescent protein (GFP) in cytochrome c oxidase, subunit VIIIa of mitochondria (Shitara et al., 2001) were obtained from Riken bio resource center, Japan. Animals were housed and bred at the Experimental Biomedicine animal facility (University of Gothenburg, Gothenburg, Sweden) under specific pathogen free conditions on a 12 hr light/dark 7 cycle with ad libitum access to standard laboratory chow (B&K, Solna, Sweden) and water. All experiments were approved by the local ethical committee at University of Gothenburg (No: 203-2014 and 32-2016) and performed according to the Guidelines for the care and use of Laboratory Animals.

2.2 | Microglial cell culture

Primary cultures of purified microglia were created from 1 to 3-day-old C57BL/6 or Cox8/EGFP mice of both sexes, as previously described (Dean et al., 2010) with minor adaptations. Following decapitation, the brain was isolated with the meninges removed and washed in ice-cold Hanks buffered salt solution (HBSS; Sigma-Aldrich, St Louis, MO) supplemented with 100 U/mL penicillin and 100 µg/mL streptomycin (Sigma-Aldrich). Forebrains were dissociated by gentle trituration in Dulbecco's modified Eagle's medium (DMEM; Sigma-Aldrich) supplemented with 20% heat-inactivated fetal bovine serum (FBS; Fischer Scientific, Goteborg, Sweden) and antibiotics. The cell suspension was passed through a 70-µm cell sieve (Falcon, Corning), plated in 75-cm² flasks with vented caps (Sarstedt, Germany) at a density of two brains/flask and cultured undisturbed for 7 days with HBSS/20% FBS/antibiotics. Medium was then replaced with HBSS/10% FBS/antibiotics, and cells were cultured for a further 7 days. Microglia were selectively detached from the flasks by shaking

(3 hr, 37°C, 250 rpm) on a rotary shaker, and the microglia cell suspension was collected and centrifuged (250g × 10 min). The media were then removed, the pellet was suspended in DMEM/2% FBS/antibiotics, and the number of cells were counted with an automated cell counter (Scepter; Millipore) and seeded into Seahorse XFe96 or 24 cell well plates (1 × 10⁵ cells per well). The purity of microglia cells was evaluated by immunocytochemical staining using antibodies against ionized calcium binding adapter molecule 1 (Iba1; 1:1000; Wako Pure Chemical Industries, Ltd., Richmond, VA) and 4',6-diamidino-2-phenylindole (DAPI) (1:1000; Sigma-Aldrich) and was routinely greater than 99%. All incubations were performed at 37°C in a humidified atmosphere containing 5% CO₂ and 95% air.

2.3 | Sample preparation for microscopy

Primary microglia cells cultured from Cox8/EGFP mice were used for mitochondrial morphology analysis. Microglia cells were washed with PBS and plated on precision cover glasses thickness No. 1.5H (tol. ±5 μm) in a 24-well plate, with 1 × 10⁵ cells per well and left to adhere overnight at 37°C in a cell culture incubator. Cells were fixed with 4% paraformaldehyde in culture media for 10 min and then mounted in ProLong Diamond antifade reagent (Life Technologies, Grand Island, NY) according to the manufacturer's instructions.

2.4 | Live cell imaging

Primary microglia cells were seeded on MatTek (MatTek, Ashland, MA) glass bottom culture dishes. Following cell adherence, cells were exposed to DMSO alone (control) or LPS 100 ng/mL for 24 hr or cells were pretreated with Mdivi-1 (25 μM; Sigma, St. Louis, MO) for 1 hr followed by LPS (100 ng/mL) exposure for 24 hr. Cells were washed gently three times with warm PBS. Furthermore, anti-bleaching live cell visualization medium (DMEMgfp-2, Evrogen) was added to the cells 30 min before imaging. Images were acquired with a Zeiss LSM 880 Airyscan super-resolution system with live cell capabilities and fitted with a fast-ASmodule (Carl Zeiss, Oberkochen, Germany). Microscopes were equipped with an environmental chamber that maintained 37°C with humidified 5% CO₂ gas during imaging.

2.5 | Super-resolution structured illumination microscopy

Super-resolution structured illumination microscopy (SR-SIM) on a Zeiss ELYRA PS.1 microscope (Carl Zeiss Microscopy, Germany) was used to yield a twofold improvement in all spatial directions (Huang, Bates, & Zhuang, 2009) beyond the classical Abbe-Rayleigh limit. GFP was imaged using a Plan-Apochromat 100×/1.4 oil objective, an excitation wavelength of 488 nm, and an emission wavelength range of 495–575 nm. The SR-SIM images were acquired as z-stacks with three angles and five phases in each plane and the z-step between planes was 3.30 nm. SR-SIM processing was performed using the Zeiss Zen software package. 3D rendering was done using Volocity 6 (Perkin-Elmer), and figures were compiled using Photoshop CC software (Adobe Systems, San Jose, CA).

2.6 | Mitochondrial morphology analysis

Primary microglia were treated with LPS, Mdivi-1, or DMSO as described previously, and mitochondria were categorized based on length: fragmented (<1 μm), tubular (1–3 μm), and elongated (>3 μm), as described previously (Jahani-Asl et al., 2011). Over 20 cells were analyzed in Control, LPS-treated, LPS plus Mdivi-1 in three independent experiments. Volocity 6 was used for 3D rendering and to quantify mitochondrial length, volume, and number.

2.7 | Measurement of oxygen consumption rate and extracellular acidification rate

Real-time measurements of oxygen consumption rates (OCRs) and extracellular acidification rates (ECARs), a measure of lactate production, were performed on an XFe96 Seahorse extracellular flux analyser (Seahorse Biosciences, North Billerica, MA). The optimal seeding density and test compound concentrations were empirically determined before initiation of experiments. According to the methods described in the XFe96 Extracellular Flux Analyzer User Manual (Seahorse Bioscience), preliminary studies were run with carbonyl cyanide-4-(trifluoromethoxy)phenylhydrazone (FCCP) to identify the optimal number of cells required to observe a sufficient shift in OCR and ECAR. Once the cell number was decided, we determined the optimal working concentrations for each of the stimulating compounds used in the mitochondrial function analysis (oligomycin, FCCP, and rotenone). Cells were then plated into XFe96 cell culture plates (Seahorse Biosciences, North Billerica, MA) at a density of 10,000/well in 80 μL of DMEM (Sigma-Aldrich, St Louis, MO). Cells were allowed to adhere overnight in a 37°C incubator with 5% CO₂. Following cell adherence, cells were exposed to a final concentration of Ultra-pure LPS 50 or 100 ng/mL (*Escherichia coli* 055: B5, Biological Laboratories, Campbell, CA) or media alone (control) for 3, 6, or 24 hr. For mitochondrial fission blocking experiments, microglia cells were pretreated with Mdivi-1 (25 μM) or DMSO for 1 hr before LPS exposure. Media (80 μL) was removed followed by the addition of 200 μL XF base media (180 μL) supplemented with 10 mM glucose, 5 mM pyruvate, and 2 mM glutamine for OCR. For ECAR, only 2 mM glutamine was added following incubation in a non-CO₂ chamber for 1 hr.

The day before the experiment, 200 μL of XF calibration media was added to the XF sensor cartridges and kept in a non-CO₂ incubator for 24 hr. XF sensor cartridges were loaded with test compounds, and OCR/ECAR measured. OCR was measured by sequential injections of oligomycin (1 μM final concentration, blocks ATP synthase to assess respiration required for ATP turnover), FCCP (carbonyl cyanide 4-trifluoromethoxy-phenylhydrazone, 2 μM final concentration, a proton ionophore uncoupler inducing maximal respiration), and rotenone plus antimycin A (1 μM final concentration of each, which completely inhibits electron transport to measure non-mitochondrial respiration).

ECAR was measured under glucose-starved microglia. Basal glycolysis rate was determined by injecting glucose at a final concentration of 10 mM. For estimating glycolytic capacity, oligomycin was injected at a final concentration of 5 μM. Finally, 2-deoxyglucose (2-DG) was injected at a final concentration of 50 mM to measure the non-glycolytic acidification. Each step had three cycles; each cycle

consisted of 3 min mixing, 2 min incubation, and 3 min measurement. All experiments were run in three replicates with 3–4 samples per replicate. Cell counts were used to normalize OCR and ECAR.

2.8 | Multiplex cytokine assay

Bio-Plex Pro Mouse Cytokine Standard 23-Plex kit (Bio-Rad) was used to measure the concentrations of cytokines/chemokines in microglia-cultured media following the manufacturer's protocol. Microglia-conditioned media was collected from microglia samples used in the OCR and ECAR experiments explained above. Samples were normalized to cell number (1×10^5 ; 1:10 in diluent buffer) and concentrations of IL-1 α , IL-1 β , IL-2, IL-3, IL-4, IL-5, IL-6, IL-9, IL-10, IL-12 (p40), IL-12 (p70), IL-13, IL-17a, eotaxin, granulocyte colony-stimulating factor (G-CSF), granulocyte macrophage colony-stimulating factor (GM-CSF), interferon-gamma (IFN- γ), KC/chemokine (C-X-C motif) ligand 1 (CXCL1), monocyte chemoattractant protein-1 (MCP-1)/chemokine (C-C motif) ligand 2 (CCL2), macrophage inflammatory protein 1 α (MIP-1 α)/CCL3, MIP-1 β /CCL4, RANTES, and TNF- α were simultaneously quantified on a Bio Plex 200 System (Bio-Rad, Sweden), and data presented as Log10 of cytokine concentrations (picograms per milliliter).

2.9 | Succinate level measurement

Microglia cells were pretreated with vehicle (DMSO), Mdivi-1 (25 μ M; Sigma, St. Louis, MO) for 1 hr or dimethyl malonate (DMM; 10 mM; Sigma, St. Louis, MO) for 3 hr before stimulation with LPS (100 ng/mL) for 24 hr. Succinate Colorimetric Assay Kit (Sigma-Aldrich Inc., St Louis, MO) was used to determine the succinate concentrations according to the manufacturer's instructions. Microglia cells (1×10^5 cells per well) were rapidly homogenized on ice in 100 μ L of ice-cold succinate assay buffer and centrifuged at 10,000g for 5 min to remove insoluble material. Then, cell homogenates were added into a 96-well plate in duplicate wells and mixed with reaction mix provided in with the kit, which results in a colorimetric product proportional to the succinate present. The resultant mixtures were further incubated at 37°C for 20 min. The succinate concentration was determined by the standard curve using spectroscopy at 450 nm wavelength.

2.10 | Measurement of mitochondrial ROS production by live cell imaging

Mitochondrial superoxide generation was assessed in live cells using MitoSOX (Molecular Probes), a fluorogenic dye that is taken up by mitochondria, where it is readily oxidized by superoxide ($O_2^{\cdot-}$). MitoSOX Red reagent is a novel fluorogenic dye specifically targeted to mitochondria in live cells. Oxidation of MitoSOX Red reagent produces red fluorescence by superoxide but not by other ROS or reactive nitrogen species-generating systems. Primary microglia cells were seeded on MatTek (MatTek, Ashland, MA) glass bottom culture dishes (1×10^5 cells/dish) and left to adhere overnight. Following treatments described above, live microglia were incubated with 5 μ M MitoSOX at 37°C for 10 min. Cells were washed gently three times with warm PBS further anti-bleaching live cell visualization medium (DMEMgfp $^{-2}$) was added to the cells 30 min before imaging. Airyscan super-resolution microscopy on a LSM

880 (Carl Zeiss Microscopy, Germany) with an onboard incubator at 37°C was used to acquire images using a 63 \times oil objective, an excitation wavelength of 488 nm. Airyscan-processing was done using the Zeiss Zen software package. MitoSox fluorescence was quantified using Volocity 6.

2.11 | Measurement of the mitochondrial membrane potential by live cell imaging

JC-1 (Molecular Probes) is a cationic dye that exhibits mitochondrial membrane potential-dependent accumulation in mitochondria, indicated by a fluorescence emission shift from green (~525 nm) to red (~590 nm). Mitochondrial depolarization is indicated by a decrease in the red to green fluorescence intensity ratio. The potential sensitive color shift is due to concentration dependent formation of red fluorescent aggregates. Primary microglia cells were seeded, incubated, and treated as above. Following LPS exposure, the media was removed and cells were incubated with JC-1 (2 μ M final concentration) at 37°C, 5% CO $_2$ for 20 min. Cells were washed gently three times with warm PBS, and further anti-bleaching live cell visualization medium (DMEMgfp $^{-2}$) was added to the cells 30 min before imaging. Images were scanned using an oil immersion, 63 \times , and 1.3 NA objective. Samples were excited at wavelength of 488 nm and emission wavelength of 547 and 617 nm. The confocal pinhole aperture was set to 50, and the voltage to the photomultiplier tubes of each channel was maintained at equal values. Illumination was limited to periods of image acquisition. Images were exactly in phase and represented the amount of monomeric and J-aggregate JC-1 fluorescence.

2.12 | Effect of Mdivi-1 in an in vivo model of inflammation-mediated damage to the preterm brain

We used a well-characterized paradigm of systemic inflammation driven neuroinflammation (Favrais et al., 2011; Krishnan et al., 2017; Van Steenwinkel et al., 2018), which is known to have effects on brain development and behavior consistent with those reported in infants and children born preterm (Ball et al., 2017; Raju, Buist, Blaisdell, Moxey-Mims, & Saigal, 2017). Experimental protocols were approved by the institutional guidelines of the Institute National de la Santé et de la Recherche Scientifique (Inserm) France. The treatments was carried out as per previously described in full (Favrais et al., 2011), with a shortened protocol described below. Assessments of gene expression were made only in male animals as female animals are not injured in this paradigm, mimicking the male predisposition to injury observed in male preterm born infants (Peacock, Marston, Marlow, Calvert, & Greenough, 2012). Briefly, mice received twice a day from P1 to P2 and once on P3 a 5- μ L intra-peritoneal (IP) injection of 10 μ g/kg/injection recombinant mouse IL-1 β in phosphate buffered saline (PBS; R&D Systems, Minneapolis, MN), or PBS alone or P1–P3 pups were co-injected with IL-1 β and 3 mg/kg/injection of Mdivi-1 (IP, 5 μ L).

2.13 | Isolation and ex vivo microglia and gene expression analysis

At P3, brains were collected for cell dissociation and CD11B+ cell separation using a magnetic coupled antibody anti-CD11B (Miltenyi, MACS Technology) as previously described in detail (Krishnan et al.,

2017; Schang et al., 2014; Shioh et al., 2017). Microglia are the predominant CD11B cell in this model of injury by more than 100-fold compared with populations of either macrophage or neutrophil (Krishnan et al., 2017). Total RNA was extracted from the CD11B+ microglia cells with the RNeasy mini kit (Qiagen, France). RNA quality and concentration were assessed by spectrophotometry (Nanodrop™, ThermoFisher Scientific, MA). Reverse transcription was achieved with the iScript™ cDNA synthesis kit (Bio-Rad, France), and RT-qPCR was performed in triplicate for each sample using SYBR Green Super-mix (Bio-Rad) as previously described (Chhor et al., 2013). Primers were designed using Primer3 plus software (see sequences in Supporting Information Table S1). Specific mRNA levels were calculated after normalization to Rpl13a mRNA (reference gene) based on previous reference gene suitability testing. The data are presented as relative mRNA units with respect to the control group (expressed as fold over control value).

2.14 | Statistics

All statistics are reported as mean ± SEM, performed using GraphPad Prism 7.0 (GraphPad Software). Significance scores are * for $p < 0.05$, ** for $p < 0.01$, *** for $p < 0.001$, and **** $p < 0.0001$.

3 | RESULTS

3.1 | LPS exposure induces excessive mitochondrial fragmentation in microglial cells

Mitochondrial morphology was examined in primary microglia cells cultured from Cox8-EGFP mice exposed to 50 or 100 ng/mL LPS

using 3D SR-SIM microscopy. The number of fragmented mitochondria was significantly increased in microglia cells stimulated with 100 ng/mL LPS for 24 hr (Figure 1c), and elongated and tubular mitochondria were decreased compared with untreated controls (Figure 1g). These findings are in line with previous studies in BV2 cells (Park et al., 2013) and primary microglia but with a higher dose of LPS (1 µg/mL) (Kato et al., 2017). There was no change in the morphology of cells stimulated with 50 ng/mL LPS for 24 hr (Figure 1b,g).

3.2 | LPS induces a switch from oxidative phosphorylation (OXPHOS) to glycolysis (metabolic reprogramming) in microglia cells

OCR and ECAR were measured in real time as measures of mitochondrial respiration and glycolysis for 50 ng/mL LPS (Figure 2a–c and i–k) and 100 ng/LPS (Figure 2o–q and w–y), respectively (Wu et al., 2007), with the Seahorse XFe96. Basal OCR and ATP-linked OCR was significantly increased in microglia cells following exposure to 50 ng/mL LPS for 6–24 hr compared with controls (Figure 2d,e). FCCP-induced maximal OCR and spare respiratory capacity (SRC) decreased, whereas leak-driven OCR significantly increased with exposure to 50 ng/mL of LPS (Figure 2f–h). The ECAR parameters (glycolysis, glycolytic capacity and glycolytic reserve) were increased following exposure to 50 ng/mL LPS for 6–24 hr compared with controls (Figure 2l–n). These results show that a moderate dose of LPS increases both OCR and glycolysis.

Exposure to 100 ng/mL of LPS for 6 hr resulted in an increase in basal OCR, ATP-linked OCR, and leak-linked OCR compared with controls (Figure 2r,s). In contrast, there was a significant decrease in basal OCR and ATP linked OCR at 24 hr after 100 ng/mL LPS (Figure 2r,s,u).

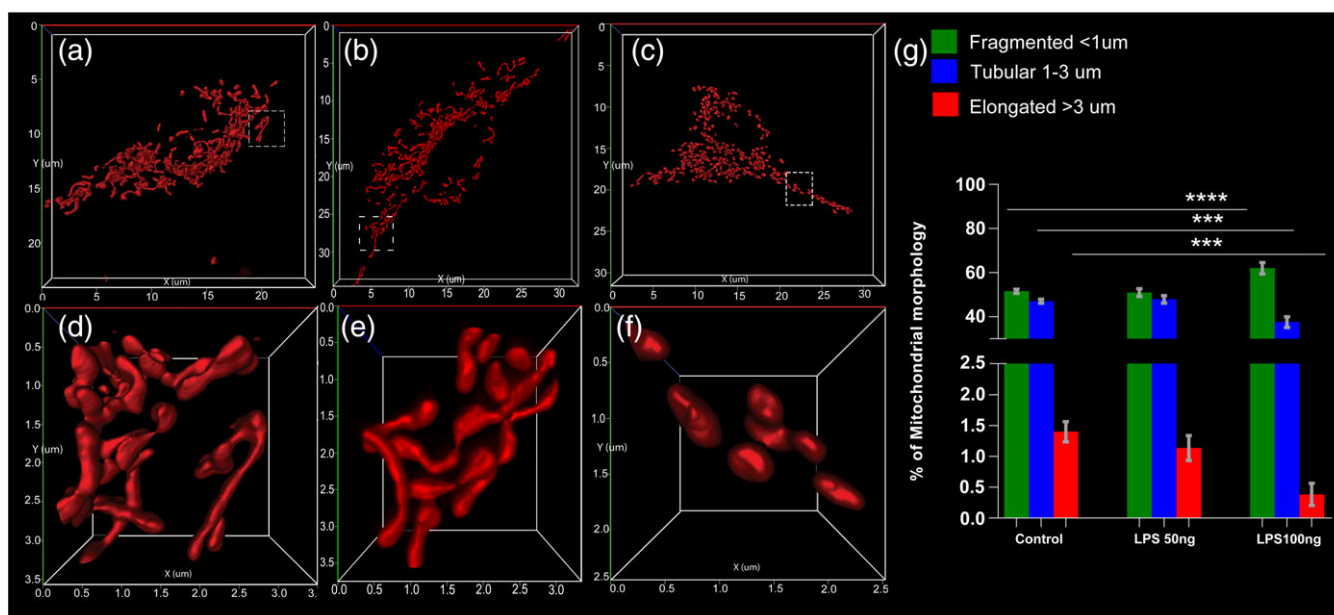


FIGURE 1 Lipopolysaccharide (LPS) induces dose-dependent mitochondrial fragmentation. Super-resolution microscopy reveals excessive mitochondrial fragmentation (a) control, (b) 50 ng/mL LPS exposure for 24 hr, (c) 100 ng/mL LPS exposure for 24 hr, (d–f) shows a higher magnification of the image in the white square in the upper panel. (g) Graphs showing results from an analysis of mitochondria morphology in primary microglia cells treated with LPS for 24 hr. The data are for at least 12 cells per condition in three independent experiments. Bar graphs expressed as mean ± SEM. *** $p \leq 0.001$; Student's *t* test calculating the difference between control and LPS treated groups [Color figure can be viewed at wileyonlinelibrary.com]

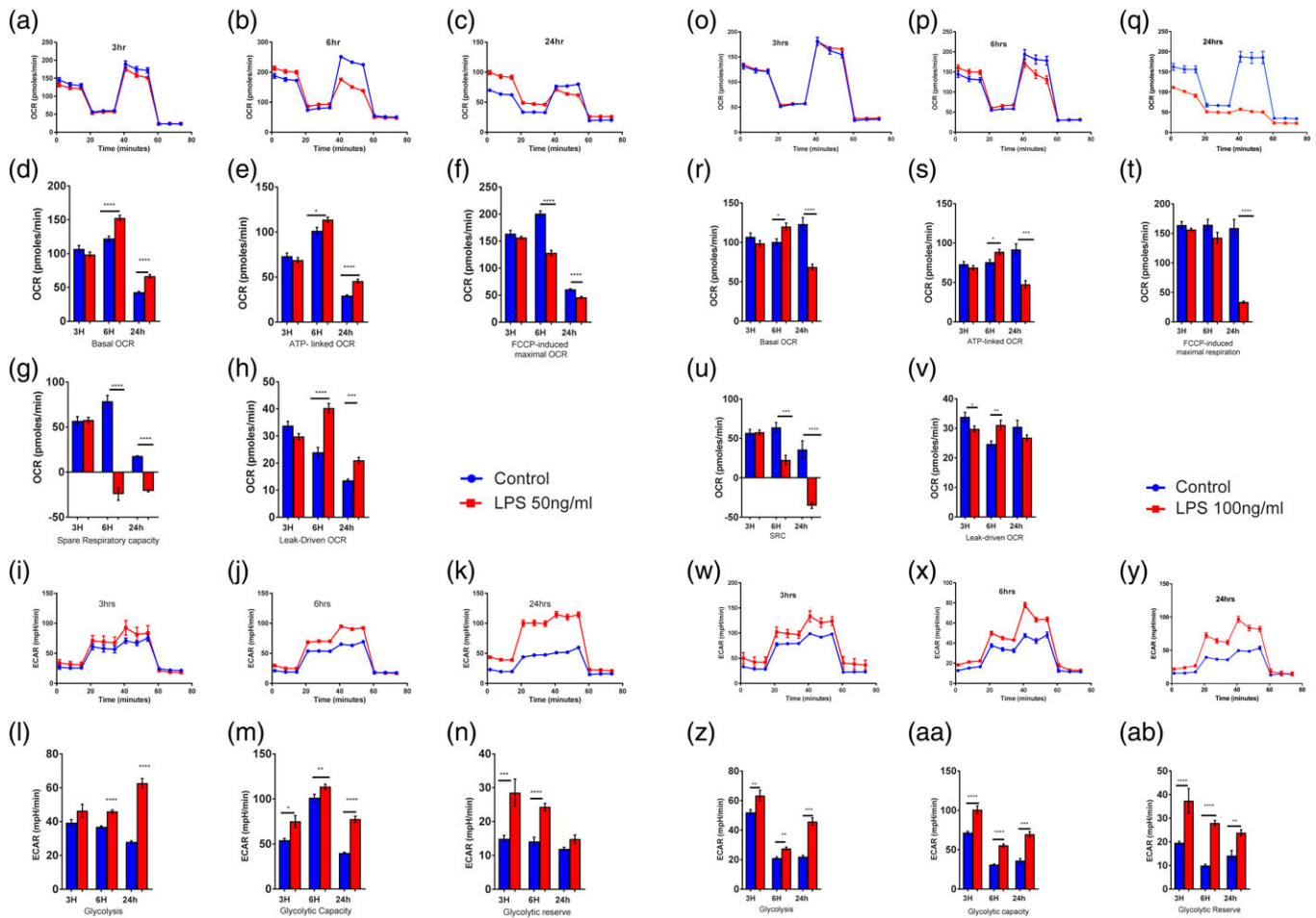


FIGURE 2 LPS dependent metabolic shift. Low dose of LPS (50 ng/mL) induces an increase in mitochondrial respiration and glycolysis: 50 ng/mL LPS treatment shows an increase in basal OCR, ATP-linked OCR (d, e), whereas FCCP-linked maximal OCR (f) and spare respiratory capacity (g) decreased from 3 to 24 hr. Leak-driven OCR was also increased from 6 to 24 hr. Glycolytic parameters, based on ECAR, tended to increase from 3 to 24 hr (i–n). Whereas a high dose (100 ng/mL) of LPS induces a time-dependent metabolic shift. 100 ng/mL LPS treatment for 6 hr shows an increase in basal OCR, ATP-linked OCR, whereas LPS treatment for 24 hr resulted in a decrease of basal and ATP-linked OCR (r, s). FCCP-linked maximal OCR (t) and spare respiratory capacity (u) decreased from 6 to 24 hr. Leak-driven OCR was increased at 6 hr (v). OCR and ECAR measured for 3, 6, and 24 hr are expressed in bar graph format as the mean \pm SEM $n = 9$. * $p \leq 0.05$; ** $p \leq 0.01$; *** $p \leq 0.001$; Student's *t*-test calculating the difference between control and LPS treated groups. LPS = lipopolysaccharide; OCR = oxygen consumption rate; FCCP = carbonyl cyanide-4-(trifluoromethoxy)phenylhydrazone; ECAR = extracellular acidification rate [Color figure can be viewed at wileyonlinelibrary.com]

FCCP-induced maximal OCR and SRC significantly decreased at 24 hr 100 ng/mL LPS (Figure 2t,u). Glycolytic parameters increased with 100 ng/mL LPS exposure for 3–24 hr compared with controls (Figure 2w–y). The overall decrease in OCR and increase in ECAR parameters with 100 ng/mL LPS for 24 hr indicates a metabolic switch from OXPHOS to glycolysis.

3.3 | Mdivi-1 treatment blocks LPS-induced mitochondrial fragmentation and ROS production

Many conserved GTPase proteins are involved in mitochondrial fusion and fission dynamics such as mitofusins (MFN1 and MFN2) and dominant optic atrophy 1 (OPA1) are needed for the fusion of mitochondrial outer and inner membranes (Song, Ghochani, McCaffery, Frey, & Chan, 2009). DRP1 and mitochondrial fission 1 protein (FIS1) are the main mitochondrial fission mediators (Frezza et al., 2006). We used the mitochondrial fission inhibitor Mdivi-1 (Ruiz, Alberdi, & Matute, 2018) as the high (100 ng/mL) dose of LPS induced an increase in

fragmented mitochondria (Figure 3b). We examined the effect of pharmacologically blocking mitochondrial fission in LPS-exposed microglia cells cultured from Cox8/EGFP mice by pretreatment with 25 μ M Mdivi-1 for 1 hr followed by incubation with LPS (100 ng/mL) for 24 hr. Results revealed that LPS-induced excessive mitochondrial fragmentation was significantly inhibited by Mdivi-1 pretreatment and normalized mitochondrial morphology (Figure 3c). Mdivi-1 treatment before LPS exposure reduced the number of fragmented mitochondria and increased the number of tubular and elongated mitochondria to control levels (Figure 3d).

3.4 | Mdivi-1 treatment normalized OCR and ECAR in the microglia cells

Because Mdivi-1 restored mitochondrial morphology, we interrogated its effect on cellular respiration and ECAR-dependent glycolysis and glycolytic capacity (Figure 4a,b,h,i). Mdivi-1 pretreatment in cells exposed to LPS (100 ng/mL for 6 hr) exhibited a decrease in the level

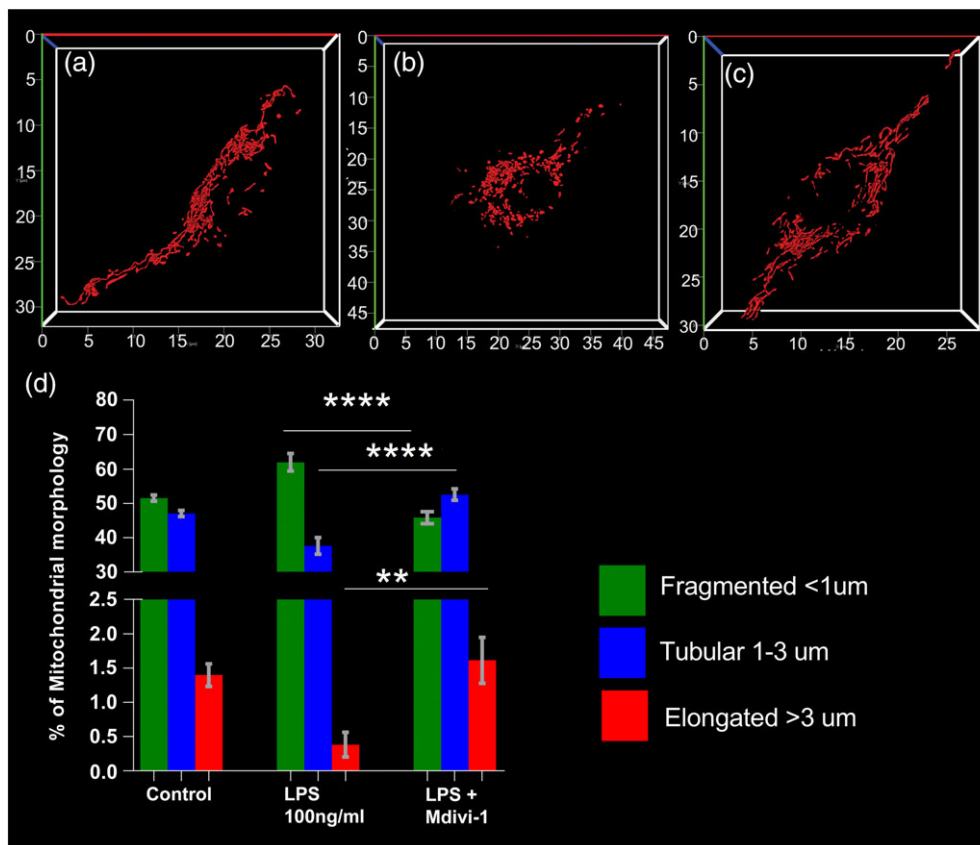


FIGURE 3 Pharmacologic blockade of DRP1 by Mdivi-1 re-established mitochondrial morphology. Mdivi-1 pretreatment (25 μ m) for 1 hr followed by LPS (100 ng/mL) exposure for 24 hr resulted in a decrease of fragmented mitochondria and an increase in tubular and elongated mitochondria (d). (a) Control cells treated with vehicle (DMSO), (b) LPS (100 ng/mL) exposure for 24 hr, (c) LPS (100 ng/mL) + Mdivi-1. Bar graphs expressed as mean \pm SEM. The data are for at least 12 cells per condition in three independent experiments. ** $p \leq 0.01$; *** $p \leq 0.001$; Student's t-test calculating the difference between LPS and LPS + Mdivi-1 groups. DRP1 = dynamin-related protein 1; LPS = lipopolysaccharide [Color figure can be viewed at wileyonlinelibrary.com]

of basal respiration and ATP-linked OCR to control levels compared with LPS treated cells (Figure 4c,d). Conversely, Mdivi-1 treatment in cells exposed to 100 ng LPS for 24 hr led to an increase in basal and ATP-linked OCR compared with non-treated LPS exposed cells (Figure 4c,d). Mdivi-1 treatment also increased FCCP-induced maximal OCR at 24 hr and leak-driven OCR compared with LPS exposed cells at both time points (Figure 4e,f). Administration of Mdivi-1 in combination with LPS normalized the spare respiratory capacity (Figure 4g). ECAR measurements showed that glycolysis and glycolytic capacity was significantly reduced to control levels in Mdivi-1 treated cells at 6 and 24 hr 100 ng/mL LPS exposure (Figure 4h-k) compared with LPS exposed cells.

3.5 | Mdivi-1 reduces the LPS induced release of cytokines and chemokines

To show how LPS activation was inducing an inflammatory reaction in the primary microglia and to test whether this was effected by Mdivi-1, we measured cytokine and chemokine response in microglia conditioned media after treatment with of LPS and or Mdivi-1 (Supporting Information Figures S1 and S2). As expected both doses of LPS led to a significant upregulation of essentially all cytokines and chemokines compared with controls. In general, there was much higher cytokine

production in microglia exposed to 100 ng-24 hr LPS conditioned media compared with 50 ng-24 hr LPS. We next determined if blockade of mitochondrial fission also modulated LPS-induced expression of cytokine and chemokine mediators. Mdivi-1 significantly reduced the pro-inflammatory cytokines (IL-1 α , IL-6, TNF- α , IL-12(p40)), chemokines (G-CSF, CCL5, RANTES), and anti-inflammatory cytokines (IL-10, IL-13) and the chemokines (monocyte chemotactic protein 1 (MCP-1 β), in response to 100 ng/mL of LPS for 24 hr. The LPS-induced production of IL-2, IL-5, and MIP1 α were not significantly reduced by Mdivi-1 (Figure 5).

3.6 | Mdivi-1 suppresses LPS-induced succinate production

Succinate is a well-established pro-inflammatory metabolite that is known to accumulate during LPS-induced macrophage activation (Mills et al., 2016), but the role of succinate during microglia activation needs further investigation. We found that LPS (100 ng/mL) resulted in a significant increase of succinate (Figure 6a) accompanying the expression of pro/anti-inflammatory cytokines and chemokines. Mdivi-1 pretreatment (Figure 6a) or blocking succinate production by succinate dehydrogenase inhibitor (DMM, 10 mM) (Figure 6b) normalized succinate production. These results were further strengthened by

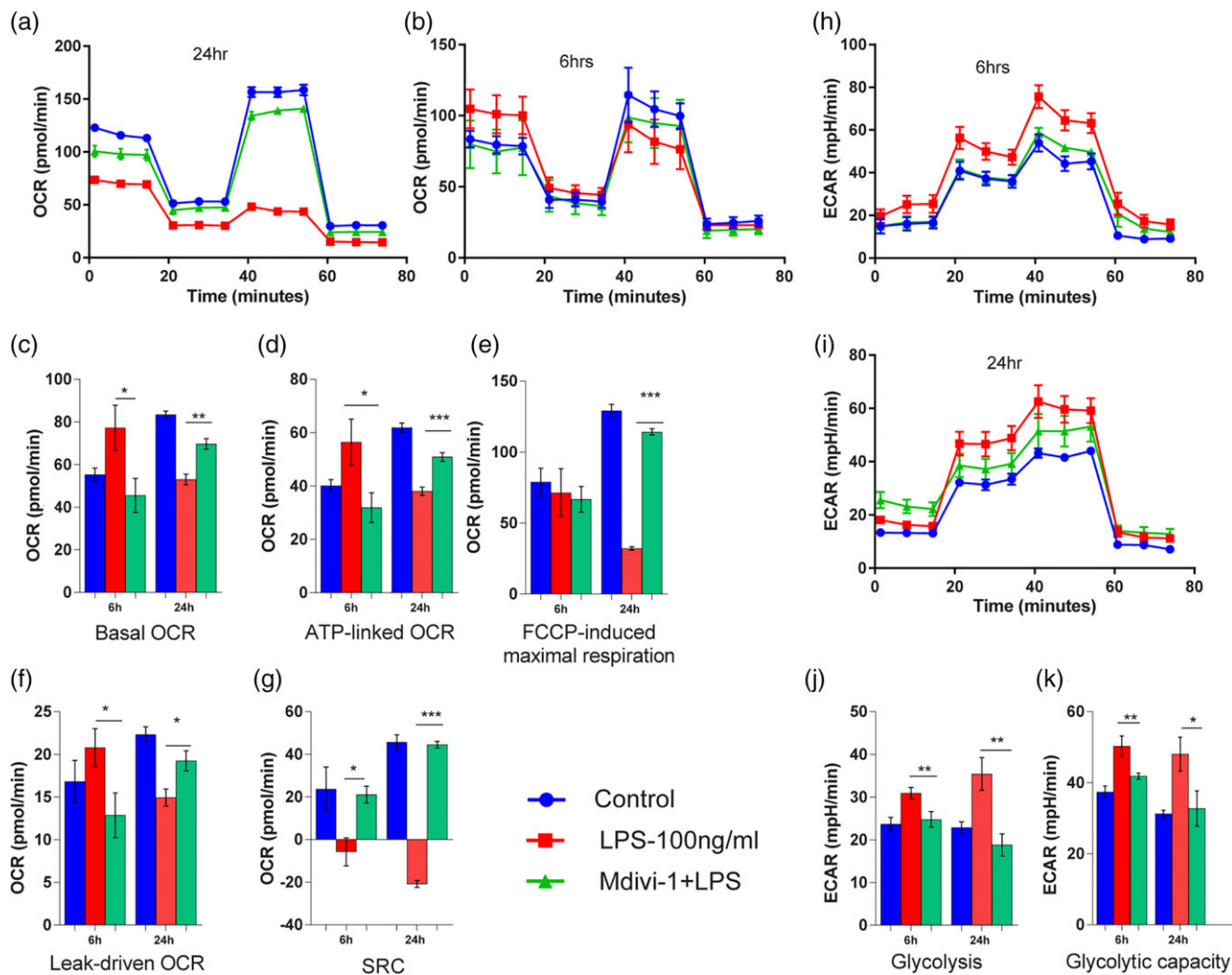


FIGURE 4 Mdivi-1 treatment reversed the metabolic shift. Inhibition of DRP1 by Mdivi-1 resulted in reduced basal OCR and ATP-linked OCR at 6 hr, whereas Mdivi-1 increased basal OCR and ATP-linked OCR at 24 hr compared with 100 ng/mL LPS exposure (c, d). LPS induced reduction in FCCP-induced maximal respiration and leak-driven OCR at 24 hr, which was normalized by Mdivi-1 (e, f). The LPS-evoked drop in SRC was prevented by Mdivi-1 (g). Mdivi-1 normalized LPS-induced increased ECAR dependent glycolysis and glycolytic capacity (j, h). OCR and ECAR measured for 3, 6, and 24 hr are expressed in bar graph format as the mean \pm SEM, $n = 6-9$. *** $p \leq 0.001$; Student's t -test calculating the difference between LPS and LPS + Mdivi-1 treated groups. DRP1 = dynamin-related protein 1; LPS = lipopolysaccharide; OCR = oxygen consumption rate; FCCP = carbonyl cyanide-4-(trifluoromethoxy)phenylhydrazone; ECAR = extracellular acidification rate; SRC = spare respiratory capacity [Color figure can be viewed at wileyonlinelibrary.com]

the fact that treatment with DMM or scavenging ROS production with NAC (10 mM, 30 min) recapitulated the effects of Mdivi-1 (Figure 5) by reducing pro/anti-inflammatory cytokines and chemokine release (Supporting Information Figure S3). Excessive fission results in fragmented mitochondria and causes a metabolic shift in microglia (Khacho et al., 2014) from OCR to ECAR. This may result in increased succinate production which in turn acts as a feedback loop to amplify aberrant mitochondrial fission (Lu et al., 2018).

3.7 | Inhibition of mitochondria fission by Mdivi-1 suppresses mitochondrial ROS production

Mitochondrial ROS plays an important role in LPS-induced immune responses (Park et al., 2015). To examine the role of ROS production after LPS stimulation, mitochondrial ROS (mtROS) was measured with MitoSOX, a mitochondrial superoxide indicator. The fluorescence

intensity of MitoSOX increased 24 hr after the LPS stimulation (100 ng/mL, 24 hr) (Figure 7). Treatment with Mdivi-1 (25 μ M, 1 hr) before LPS exposure abolished the increase in MitoSOX fluorescence intensity observed 2 hr after the LPS stimulation. These results indirectly show that that mitochondrial fission (induced by TLR4 stimulation) increases ROS production as shown in this study and others (Katoh et al., 2017; Park et al., 2013).

3.8 | Mdivi-1 treatment attenuated LPS induced increase of mitochondrial membrane potential

Our data suggest that after LPS (100 ng/mL) exposure for 24 hr microglia mainly depended on glycolysis for energy production. Therefore, we investigated the mitochondrial membrane potential using the mitochondrial membrane potential probe JC-1 in these conditions. We found that there was a consequent elevation of mitochondrial

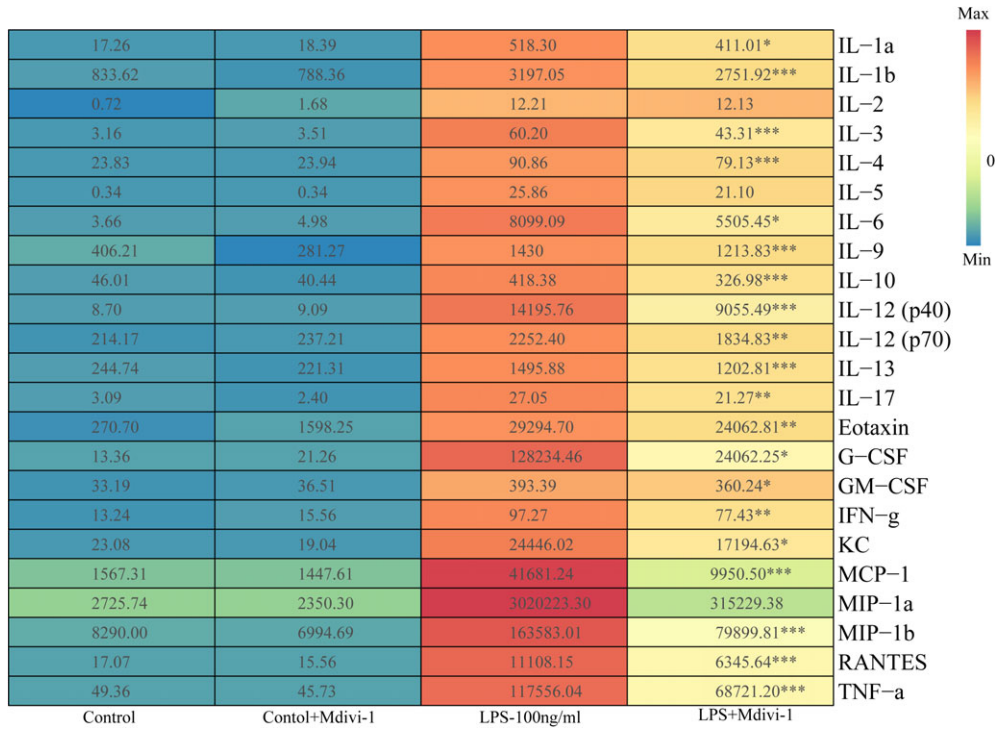


FIGURE 5 Mdivi-1 treatment abolished lipopolysaccharide (LPS) induced exaggerated pro/anti-inflammatory cytokine and chemokine response. Microglia cells were pretreated with Mdivi-1 (25 μM) for 1 hr followed by LPS (100 ng/mL) for 24 hr, and microglial cells were collected and analyzed by 23-plex cytokine assay. Heat maps show cytokine concentration (pg/mL). KC = keratinocyte chemoattractant. *n* = 8 **p* ≤ 0.05; ***p* ≤ 0.01; ****p* ≤ 0.001; Student's *t*-test calculating the difference between LPS and LPS + Mdivi-1 treated groups [Color figure can be viewed at wileyonlinelibrary.com]

membrane potential and treatment with Mdivi-1 significantly reduced mitochondrial membrane potential (525/565 nm) ratio compared with LPS treated group (Figure 8).

3.9 | Mdivi-1 treatment attenuated microglial activation in a mouse paradigm of neuroinflammation

Based on our working hypothesis that Mdivi-1 can reduce the inflammatory reaction of microglia, we sought to investigate the potential for Mdivi-1 to reduce the activation of microglia in vivo (Favrais et al., 2011; Krishnan et al., 2017). We isolated microglia from the brains of

animals at P3 following induction of systemically driven neuroinflammation and con-current treatment with Mdivi-1 from P1 to P3. We analyzed the isolated microglia for gene expression of markers associated with functional phenotypes including cytotoxic (*Nos2*, *Ptgs2*, *Cd32*), repair and regeneration (*Arg1*, *Lga3*, *Igf1*), and immunomodulatory (*Il1ra*, *Il4a*, *Socs3*) phenotypes. Exposure to neuroinflammatory-stimuli affected the gene expression as expected (Krishnan et al., 2017), with increased expression of all of the genes except for the gene for IGF1, which was decreased. IGF1 is a pleiotropic growth factor necessary for myelogenesis and known to be decreased by pro-inflammatory microglial activation (Włodarczyk et al., 2017). Mdivi-1

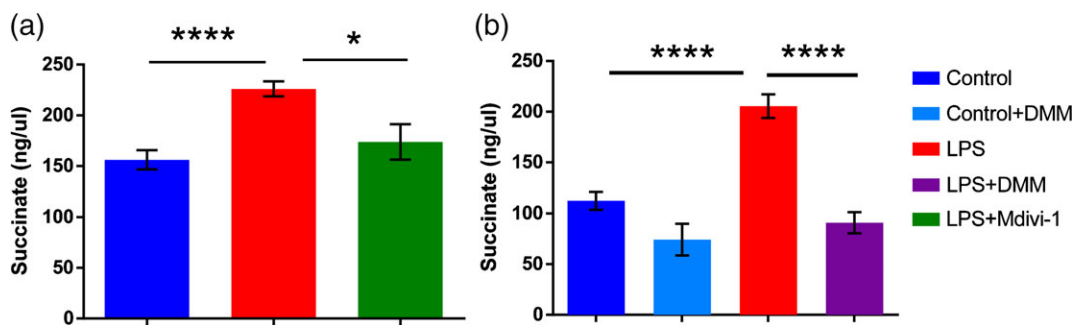


FIGURE 6 (a) Mdivi-1 normalized lipopolysaccharide (LPS) induced succinate upregulation. Microglia cell homogenates of cells were analyzed by succinate colorimetric assay. Microglia cells were pretreated with Mdivi-1 (25 μM; 1 hr) followed by LPS exposure of 100 ng LPS for 24 hr resulted in significant downregulation of LPS induced succinate upregulation. Bar graph expressed as the mean ± SEM, *n* = 8. **p* ≤ 0.05; Student's *t*-test calculating the difference between LPS and LPS + Mdivi-1 treated groups. (b) Succinate dehydrogenase inhibitor recapitulated the effects of Mdivi-1. Pretreatment with dimethyl malonate (DMM, 10 mM; 3 hr) before LPS exposure attenuated succinate accumulation. Bar graph format as the mean ± SEM, *n* = 9. **p* ≤ 0.05, Tukey's post hoc test using one-way ANOVA revealed difference between control, control + DMM, LPS, and LPS + DMM treated groups [Color figure can be viewed at wileyonlinelibrary.com]

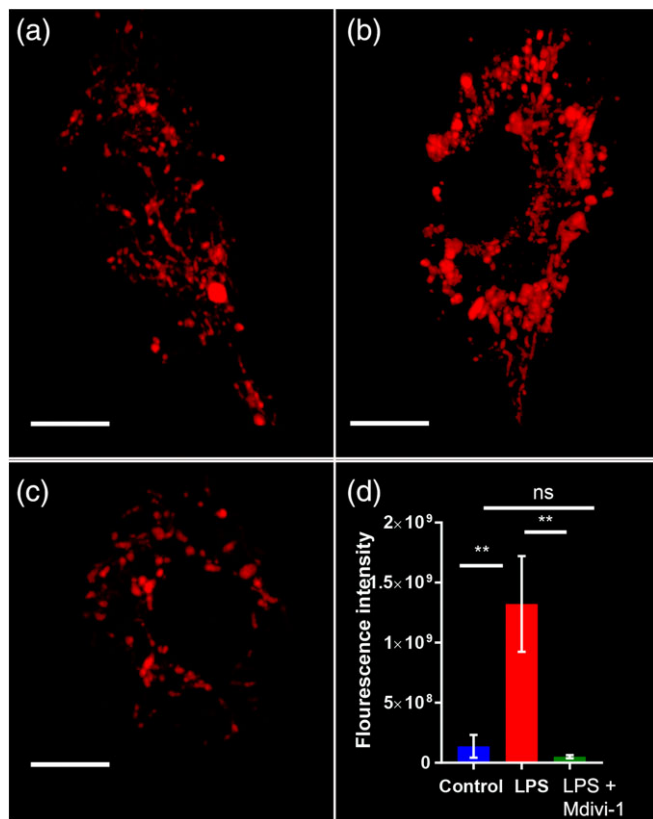


FIGURE 7 Mdivi-1 treatment abolished lipopolysaccharide (LPS)-induced mitochondrial reactive oxygen species production. (a) Control, (b) 100 ng/mL LPS exposure for 24 hr, (c) LPS + Mdivi-1, (d) graphs showing results from an analysis of mitosox fluorescence by live cell airyscan microscopy. The data are for at least 12 cells per condition in three independent experiments. Bar graphs expressed as mean \pm SEM. ** $p \leq 0.01$; Student's *t*-test calculating the difference between control LPS and Mdivi-1 treated groups [Color figure can be viewed at wileyonlinelibrary.com]

treatment normalized to control (PBS) levels the expression of genes associated with cytotoxicity and immunomodulation, but had no effect on IGF1 gene expression, and only partly recovered Galectin-3 gene expression (*Lgal3*), indicating that exposure to Mdivi-1, which inhibits mitochondrial fragmentation, modulates the microglial inflammatory response also in vivo (Figure 9).

4 | DISCUSSION

This study strengthens our knowledge of the links between mitochondrial architecture, inflammation, and energy metabolism in microglial cells. We have shown that activation of microglia to a pro-inflammatory activation state increased mitochondrial fragmentation, which was accompanied by a reduction in oxidative phosphorylation and an increase in glycolysis, which was dose and time dependent. Pretreatment with the putative mitochondrial division inhibitor, Mdivi-1, normalized LPS-induced mitochondrial fragmentation, normalized the cellular respiration and glycolysis to control levels. Mdivi-1 greatly reduced LPS-induced cytokine production normalized LPS-induced ROS production and mitochondrial membrane potential.

Neuroinflammation includes complex changes in microglial phenotypes, mediated by gene expression changes leading to the production of cytokines and chemokines and production of ROS. Altogether this triggers oxidative and nitrosative stress in the brain (Bolouri et al., 2014; Hellström Erkenstam et al., 2016). We observed as expected that LPS-activated microglia produced a plethora of chemokines and cytokines and ROS. In this pro-inflammatory scenario, suppression of LPS-induced mitochondrial ROS plays a role in modulating the production of pro-inflammatory mediators by preventing MAPK and NF- κ B activation suggesting a potential therapy for inflammation-associated degenerative neurological diseases (Park et al., 2015).

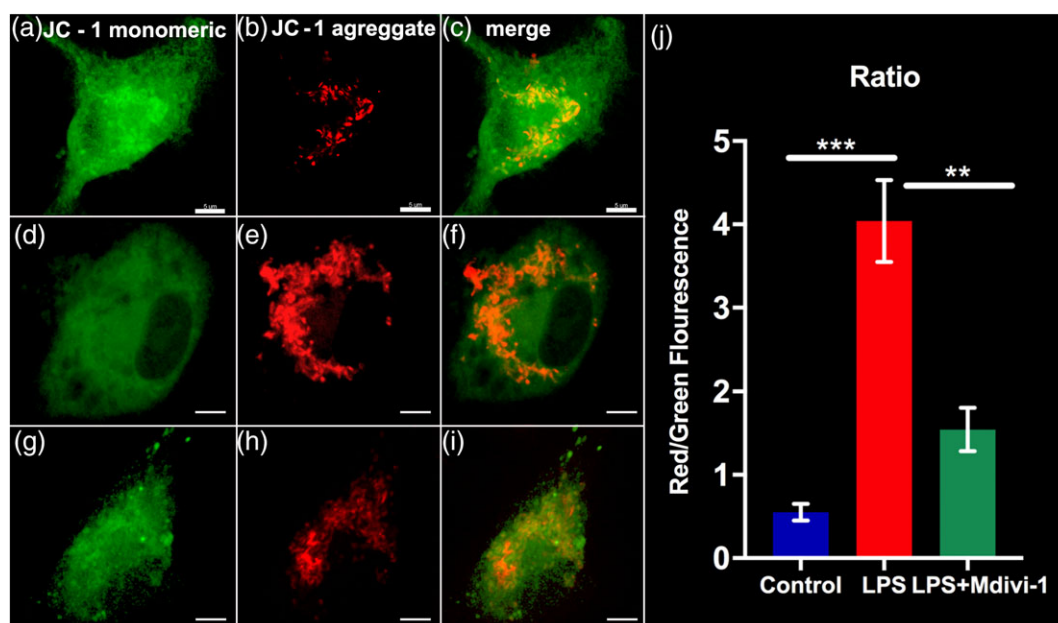


FIGURE 8 Mdivi-1 treatment attenuated lipopolysaccharide (LPS) induced increase of mitochondrial membrane potential: (a–c) control, (d, f) 100 ng/mL LPS exposure for 24 hr, (g, i) LPS + Mdivi-1. Graphs showing results from an analysis of JC1 fluorescence 525/565 nm by live cell airyscan microscopy. The data are for at least six cells per condition in three independent experiments. Bar graphs expressed as mean \pm SEM. ** $p \leq 0.01$, *** $p \leq 0.001$, Student's *t*-test [Color figure can be viewed at wileyonlinelibrary.com]

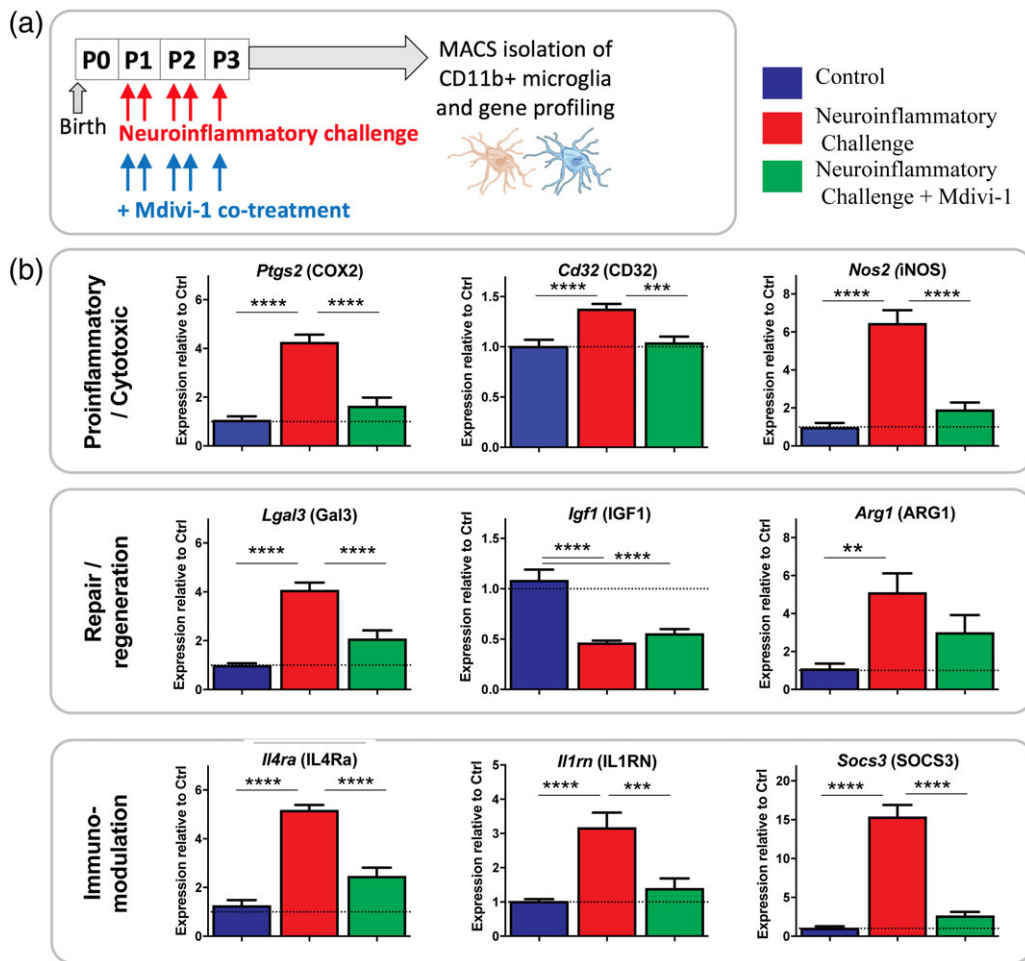


FIGURE 9 (a) Schematic representation of the testing of the effects of Mdivi-1 on neuroinflammation induced microglial gene expression in vivo. (b) Mdivi-1 prevented many of the neuroinflammation (IL-1 β -induced) alterations in gene expression. Relative gene expression of *Ptgs2*, *Cd32*, *Nos2*, *Lgal3*, *Igf1*, *Arg1*, *Il4ra*, *Il1rn*, and *Socs3* were assessed by qRT-PCR from MACS isolated CD11b + microglia from P3 mice. Protein names for the genes are shown in brackets on the panels. The legend indicates that the first bar (blue) is the control (PBS injected group), the middle bar (red) is the neuroinflammatory challenge group, and that the right bar (green) is the group challenged with neuroinflammation but also treated with Mdivi-1. The dotted line highlights the gene expression in the control group. Results are expressed as the mean \pm SEM. There are 10–15 data points from three independent experiments per group. Data were analyzed with a Kruskal–Wallis ANOVA, $p < 0.001$ with a Dunn's test for comparison among groups: ** $p < 0.01$, *** $p < 0.001$, **** $p < 0.0001$ [Color figure can be viewed at wileyonlinelibrary.com]

To understand LPS-induced changes in mitochondrial structure, we used high-resolution 3D ELYRA-SIM (Shim et al., 2012) to quantify mitochondrial morphology which revealed that high-dose LPS for 24 hr increased fragmentation. A low dose of LPS caused an initial increase in OCR which was not accompanied by any change in mitochondrial morphology. However, a higher dose of LPS induced a decrease of OCR and a further increase of ECAR accompanied by mitochondrial fission. Fragmented mitochondria constitute the preferred morphological state when respiratory activity is low (Westermann, 2012). A high or moderate dose of LPS caused a decrease in respiration, and cells became dependent on glycolysis favoring excessive fragmentation. The molecular mechanisms behind this response is not known, but it has been proposed that the energy depletion elicits mitochondrial fragmentation and subsequent mitophagy (Youle & van der Bliek, 2012). Increased mitochondrial fragmentation due to excessive fission can exacerbate the inflammatory response of microglia (Ho et al., 2018) through modulation of DRP1 de-phosphorylation and elimination of ROS (Park et al., 2016). We

chose to use Mdivi-1, a mitochondrial division inhibitor, to study microglial metabolism as it related to mitochondrial morphology as previous studies revealed that LPS exposure in microglia cells leads to activation of mitochondrial fission protein DRP1 (Katoh et al., 2017; Park et al., 2013).

Mdivi-1 is a widely accepted DRP-1 mediated mitochondrial fission inhibitor used in many studies (Baek et al., 2017; Peiris-Pagès, Bonuccelli, Sotgia, & Lisanti, 2018; So, Hsing, Liang, & Wu, 2012; Xie et al., 2013). Our data supports the assertion that changes in mitochondrial dynamics may be needed for the expression of inflammatory mediators in activated microglia cells. Mdivi-1 has previously been shown to attenuate LPS-induced ROS and pro-inflammatory mediator production in a BV-2 microglial cell line (Park et al., 2013) with a very high dose of 1 μ g/mL. BV2 cells are similar to primary microglia (Henn et al., 2009), but they contain oncogenes that render them phenotypically different with regard to, for example, proliferation and adhesion (Horvath, Nutile-McMenemy, Alkatis, & Deleo, 2008). Our findings not only show that pretreatment with Mdivi-1 reduced LPS-induced



mitochondrial fragmentation and expression of pro-inflammatory mediators but also normalized mitochondrial function in microglia. These data support the suggestion that increasing the fusion/fission ratio reduces the extent of neuroinflammation (Kim, Lee, Park, Kim, & Roh, 2016). To further support the potential validity of targeting fission as a therapeutic strategy, we tested the ability of Mdivi-1 to modify microglial activity *in vivo*. We used a paradigm of systemically driven neuroinflammation, wherein an IP injection of the inflammatory agent interleukin-1 β induces a highly complex neuroinflammatory reaction involving microglia (Krishnan et al., 2017; Van Steenwinckel et al., 2018). Supporting our *in vitro* data mdivi-1 was able to reduce the expression of genes associated with classically pro-inflammatory genes and the anti-inflammatory activation state, which is associated with the *in vivo* inflammatory reaction.

Previous work with BV2 demonstrated that LPS causes an inhibition of OXPHOS (Voloboueva, Emery, Sun, & Giffard, 2013). However, this study used a very high dose of LPS (1 μ g/mL) which is shown to elicit mitochondrial toxicity (Ahn et al., 2012). We demonstrate for the first time that a low or moderate dose of LPS (50 ng/mL) results in an increase of ATP-linked OCR and basal respiration in support of another study in skeletal muscle cells where they used a very low dose of LPS in isolated mitochondria (Frisard et al., 2015). High dose of LPS (100 ng/mL) caused a decrease in FCCP-induced maximal respiration and an increase in leak-driven respiration. A depletion of spare respiratory capacity was found at 6 and 24 hr following LPS exposure. However, we have noted no significant difference in cell viability or death after LPS.

OCR exhibited a biphasic response characterized initially by an increase of OCR in response to low LPS and then a marked drop of OCR after moderate to high doses of LPS, whereas ECAR increased in proportion to the dose of LPS. We interpret the initial increase of OCR as a means to match an increased demand of ATP. However, as the pro-inflammatory stimulus becomes stronger, it appears favorable to shift from mitochondrial respiration to aerobic glycolysis (Warburg effect) to promote more rapid ATP production (Kelly & O'Neill, 2015; Orihuela et al., 2016) and synthesis of inflammatory mediators such as cytokines/chemokines and ROS (Kelly & O'Neill, 2015). We believe the Warburg effect is an important concept for understanding metabolic changes occurring during microglial activation. It is shown that also activation of macrophages or DCs with LPS induces a metabolic switch from OXPHOS to glycolysis (Krawczyk et al., 2010). Metabolic shift may be facilitated by increased mitochondrial fission and/or reduced fusion mediated by DRP1 activation (Baker, Maitra, Geng, & Li, 2014). However, as glycolysis is less efficient at producing ATP than OXPHOS, this metabolic reorientation cannot solely be to meet energy demands. Glycolysis may also facilitate cytokine production by producing intermediate metabolites (Mills et al., 2016). A previous study found that glycolysis was required to produce optimal IFN- γ during T cell activation and is translationally regulated by the binding of the glycolysis enzyme GAPDH to IFN- γ mRNA (Chang et al., 2013).

Our results in microglia add to what has already been shown in DCs and macrophages (Williams & O'Neill, 2018), specifically that pro-inflammatory activation resulted in increased succinate accumulation. In DCs and macrophages, this succinate accumulation was related to an altered Krebs cycle and this was normalized by Mdivi-1. Aberrant

mitochondrial fission alters the Krebs cycle, by interfering with the processes after citrate and after succinate (Jha et al., 2015) by reducing of cytochrome c oxidase and succinate dehydrogenase activity (Zhang et al., 2013). Impaired succinate dehydrogenase activity results in succinate accumulation due to impaired succinate to fumarate conversion (Mills et al., 2016). Accumulated succinate drives reverse electron transport (RET) to generate excessive mitochondrial ROS production (Chouchani et al., 2014; Niatsetskeya et al., 2012). Our data support this link between accumulation of succinate and ROS production, which was prevented by Mdivi-1.

LPS induced an increase in proton leak with an increase in membrane potential. Proton leak is partly mediated by uncoupling proteins (UCPs) present in the mitochondrial inner membrane (Hass & Barnstable, 2016; Krauss, Zhang, & Lowell, 2005). It is shown that in primary microglia LPS induces an increase in UCP2 levels and membrane potential. UCP2-silenced microglia stimulated with LPS show a decrease in membrane potential (De Simone et al., 2015). In macrophages LPS stimulation repurpose their mitochondria from ATP production to succinate-dependent ROS generation, with glycolysis taking on the role of ATP generation. In this case, mitochondria sustain a high membrane potential because protons generated by the electron transport chain to make ATP are no longer being consumed by mitochondrial ATP synthase (Mills et al., 2016). Macrophages can also reorganize their respiratory chain in response to a bacterial infection, decreasing Complex I levels and increasing the activity of Complex II (Garaude et al., 2016). These changes boost production of pro-inflammatory cytokines such as interleukin 1 β (IL-1 β). Our data support these findings as normalizing mitochondrial membrane potential and ROS production with Mdivi-1 abolished pro- and anti-inflammatory cytokine and chemokine release.

Aberrant activation of microglial affects neurodegenerative processes through various neurotoxic cascades. We have shown that pro-inflammatory microglial activation alters cellular bioenergetics by inducing mitochondrial dysfunction and promoting a switch to glycolysis, supported by excessive mitochondrial fragmentation, and increased cytokine output. This is likely an adaptive mechanism as the transition of sensing and surveying microglia into an activated state is likely to be accompanied by significantly increased energy consumption. Preventing excessive mitochondrial fission in microglial cells stimulated with LPS using a fission inhibitor Mdivi-1 normalizes mitochondrial respiration and glycolysis and attenuates the release of cytokines/chemokines. These lines of *in vitro* morphological and functional data and the *in vivo* data suggest that regulating mitochondrial dynamics may be a useful therapeutic modality for preventing neurological disorders caused by aberrant microglia activation.

ACKNOWLEDGMENTS

We gratefully acknowledge the support from ERA-net (EU; VR 529-2014-7551), Wellcome Trust (WT094823), the Medical Research Council, Swedish Medical Research Council (VR 2015-02493, HH; VR 2012-2992, CM), Brain Foundation (HH, CM), Ahlen Foundation (HH, CM, SN), ALF-GBG (426401, HH; 432291, CM), and the Leducq Foundation (DSRRP34404), Torsten Söderberg (M98/15, CM), Fri-murare Barnhusdirektionen (SN), to enable this study to be completed.

In addition, the authors acknowledge financial support from the Department of Health via the National Institute for Health Research (NIHR) comprehensive Biomedical Research Centre Award to Guy's & St Thomas' NHS Foundation Trust in partnership with King's College London and King's College Hospital NHS Foundation Trust. Centre for Cellular Imaging at the University of Gothenburg and the National Microscopy Infrastructure, NMI (VR-RFI 2016-00968) for providing assistance in microscopy.

CONFLICT OF INTEREST

We report no conflict of interest.

ORCID

Syam Nair  <https://orcid.org/0000-0001-8470-2162>

REFERENCES

- Ahn, S. K., Hong, S., Park, Y. M., Choi, J. Y., Lee, W. T., Park, K. A., & Lee, J. E. (2012). Protective effects of agmatine on lipopolysaccharide-injured microglia and inducible nitric oxide synthase activity. *Life Sciences*, *91*(25), 1345–1350. <https://doi.org/10.1016/j.lfs.2012.10.010>
- Baek, S. H., Park, S. J., Jeong, J. I., Kim, S. H., Han, J., Kyung, J. W., ... Jo, D. G. (2017). Inhibition of Drp1 ameliorates synaptic depression, abeta deposition, and cognitive impairment in an Alzheimer's disease model. *The Journal of Neuroscience*, *37*(20), 5099–5110. <https://doi.org/10.1523/jneurosci.2385-16.2017>
- Baker, B., Maitra, U., Geng, S., & Li, L. (2014). Molecular and cellular mechanisms responsible for cellular stress and low-grade inflammation induced by a super-low dose of endotoxin. *The Journal of Biological Chemistry*, *289*(23), 16262–16269. <https://doi.org/10.1074/jbc.M114.569210>
- Ball, G., Aljabar, P., Nongena, P., Kennea, N., Gonzalez-Cinca, N., Falconer, S., ... Edwards, A. D. (2017). Multimodal image analysis of clinical influences on preterm brain development. *Annals of Neurology*, *82*, 233–246. <https://doi.org/10.1002/ana.24995>
- Bolouri, H., Savman, K., Wang, W., Thomas, A., Maurer, N., Dullaghan, E., ... Mallard, C. (2014). Innate defense regulator peptide 1018 protects against perinatal brain injury. *Annals of Neurology*, *75*(3), 395–410. <https://doi.org/10.1002/ana.24087>
- Buck, M. D., O'Sullivan, D., Klein Geltink, R. I., Curtis, J. D., Chang, C. H., Sanin, D. E., ... Pearce, E. L. (2016). Mitochondrial dynamics controls T cell fate through metabolic programming. *Cell*, *166*(1), 63–76. <https://doi.org/10.1016/j.cell.2016.05.035>
- Butovsky, O., & Weiner, H. L. (2018). Microglial signatures and their role in health and disease. *Nature Reviews. Neuroscience*, *19*, 622–635. <https://doi.org/10.1038/s41583-018-0057-5>
- Cassidy-Stone, A., Chipuk, J. E., Ingeman, E., Song, C., Yoo, C., Kuwana, T., ... Nunnari, J. (2008). Chemical inhibition of the mitochondrial division dynamin reveals its role in Bax/Bak-dependent mitochondrial outer membrane permeabilization. *Developmental Cell*, *14*(2), 193–204. <https://doi.org/10.1016/j.devcel.2007.11.019>
- Chang, C. H., Curtis, J. D., Maggi, L. B., Jr., Faubert, B., Villarino, A. V., O'Sullivan, D., ... Pearce, E. L. (2013). Posttranscriptional control of T cell effector function by aerobic glycolysis. *Cell*, *153*(6), 1239–1251. <https://doi.org/10.1016/j.cell.2013.05.016>
- Chhor, V., Le Charpentier, T., Lebon, S., Ore, M. V., Celador, I. L., Jossierand, J., ... Fleiss, B. (2013). Characterization of phenotype markers and neuronotoxic potential of polarised primary microglia in vitro. *Brain, Behavior, and Immunity*, *32*, 70–85. <https://doi.org/10.1016/j.bbi.2013.02.005>
- Chouchani, E. T., Pell, V. R., Gaude, E., Aksentijević, D., Sundier, S. Y., Robb, E. L., ... Murphy, M. P. (2014). Ischaemic accumulation of succinate controls reperfusion injury through mitochondrial ROS. *Nature*, *515*(7527), 431–435. <https://doi.org/10.1038/nature13909>
- De Simone, R., Ajmone-Cat, M. A., Pandolfi, M., Bernardo, A., De Nuccio, C., Minghetti, L., & Visentin, S. (2015). The mitochondrial uncoupling protein-2 is a master regulator of both M1 and M2 microglial responses. *Journal of Neurochemistry*, *135*(1), 147–156. <https://doi.org/10.1111/jnc.13244>
- Dean, J. M., Wang, X., Kaindl, A. M., Gressens, P., Fleiss, B., Hagberg, H., & Mallard, C. (2010). Microglial MyD88 signaling regulates acute neuronal toxicity of LPS-stimulated microglia in vitro. *Brain, Behavior, and Immunity*, *24*(5), 776–783. <https://doi.org/10.1016/j.bbi.2009.10.018>
- Everts, B., Amiel, E., Huang, S. C.-C., Smith, A. M., Chang, C.-H., Lam, W. Y., ... Pearce, E. J. (2014). TLR-driven early glycolytic reprogramming via the kinases TBK1-IKKe supports the anabolic demands of dendritic cell activation. *Nature Immunology*, *15*(4), 323–332. <https://doi.org/10.1038/ni.2833>
- Favrais, G., van de Looij, Y., Fleiss, B., Ramanantsoa, N., Bonnin, P., Stoltenberg-Didinger, G., ... Gressens, P. (2011). Systemic inflammation disrupts the developmental program of white matter. *Annals of Neurology*, *70*(4), 550–565. <https://doi.org/10.1002/ana.22489>
- Frezza, C., Cipolat, S., Martins de Brito, O., Micaroni, M., Beznoussenko, G. V., Rudka, T., ... Scorrano, L. (2006). OPA1 controls apoptotic cristae remodeling independently from mitochondrial fusion. *Cell*, *126*(1), 177–189. <https://doi.org/10.1016/j.cell.2006.06.025>
- Frisard, M. I., Wu, Y., McMillan, R. P., Voelker, K. A., Wahlberg, K. A., Anderson, A. S., ... Hulver, M. W. (2015). Low levels of lipopolysaccharide modulate mitochondrial oxygen consumption in skeletal muscle. *Metabolism: Clinical and Experimental*, *64*(3), 416–427. <https://doi.org/10.1016/j.metabol.2014.11.007>
- Garaude, J., Acin-Perez, R., Martinez-Cano, S., Enamorado, M., Ugolini, M., Nistal-Villan, E., ... Sancho, D. (2016). Mitochondrial respiratory-chain adaptations in macrophages contribute to antibacterial host defense. *Nature Immunology*, *17*(9), 1037–1045. <https://doi.org/10.1038/ni.3509>
- Gimeno-Bayon, J., Lopez-Lopez, A., Rodriguez, M. J., & Mahy, N. (2014). Glucose pathways adaptation supports acquisition of activated microglia phenotype. *Journal of Neuroscience Research*, *92*(6), 723–731. <https://doi.org/10.1002/jnr.23356>
- Greter, M., Lelios, I., & Croxford, A. L. (2015). Microglia versus myeloid cell nomenclature during brain inflammation. *Frontiers in Immunology*, *6*, 249. <https://doi.org/10.3389/fimmu.2015.00249>
- Hackenbrock, C. R. (1966). Ultrastructural bases for metabolically linked mechanical activity in mitochondria. I. Reversible ultrastructural changes with change in metabolic steady state in isolated liver mitochondria. *The Journal of Cell Biology*, *30*(2), 269–297.
- Hagberg, H., Mallard, C., Rousset, C. I., & Thornton, C. (2014). Mitochondria: hub of injury responses in the developing brain. *Lancet Neurology*, *13*(2), 217–232. [https://doi.org/10.1016/s1474-4422\(13\)70261-8](https://doi.org/10.1016/s1474-4422(13)70261-8)
- Hass, D. T., & Barnstable, C. J. (2016). Uncoupling protein 2 in the glial response to stress: Implications for neuroprotection. *Neural Regeneration Research*, *11*(8), 1197–1200. <https://doi.org/10.4103/1673-5374.189159>
- Hellström Erkenstam, N., Smith, P. L. P., Fleiss, B., Nair, S., Svedin, P., Wang, W., ... Mallard, C. (2016). Temporal characterization of microglia/macrophage phenotypes in a mouse model of neonatal hypoxic-ischemic brain injury. *Frontiers in Cellular Neuroscience*, *10*, 286. <https://doi.org/10.3389/fncel.2016.00286>
- Henn, A., Lund, S., Hedtjarn, M., Schratzenholz, A., Porzgen, P., & Leist, M. (2009). The suitability of BV2 cells as alternative model system for primary microglia cultures or for animal experiments examining brain inflammation. *ALTEX*, *26*(2), 83–94.
- Ho, D. H., Je, A. R., Lee, H., Son, I., Kweon, H. S., Kim, H. G., & Seol, W. (2018). LRRK2 kinase activity induces mitochondrial fission in microglia via Drp1 and modulates neuroinflammation. *Experimental Neurobiology*, *27*(3), 171–180. <https://doi.org/10.5607/en.2018.27.3.171>
- Horvath, R. J., Nutile-McMenemy, N., Alkaitis, M. S., & Deleo, J. A. (2008). Differential migration, LPS-induced cytokine, chemokine, and NO expression in immortalized BV-2 and HAPI cell lines and primary microglial cultures. *Journal of Neurochemistry*, *107*(2), 557–569. <https://doi.org/10.1111/j.1471-4159.2008.05633.x>
- Huang, B., Bates, M., & Zhuang, X. (2009). Super resolution fluorescence microscopy. *Annual Review of Biochemistry*, *78*, 993–1016. <https://doi.org/10.1146/annurev.biochem.77.061906.092014>



- Jahani-Asl, A., Pilon-Larose, K., Xu, W., MacLaurin, J. G., Park, D. S., McBride, H. M., & Slack, R. S. (2011). The mitochondrial inner membrane GTPase, optic atrophy 1 (Opa1), restores mitochondrial morphology and promotes neuronal survival following excitotoxicity. *The Journal of Biological Chemistry*, 286(6), 4772–4782. <https://doi.org/10.1074/jbc.M110.167155>
- Jha, A. K., Huang, S. C.-C., Sergushichev, A., Lampropoulou, V., Ivanova, Y., Loginicheva, E., ... Artyomov, M. N. (2015). Network integration of parallel metabolic and transcriptional data reveals metabolic modules that regulate macrophage polarization. *Immunity*, 42(3), 419–430. <https://doi.org/10.1016/j.immuni.2015.02.005>
- Katoh, M., Wu, B., Nguyen, H. B., Thai, T. Q., Yamasaki, R., Lu, H., ... Ohno, N. (2017). Polymorphic regulation of mitochondrial fission and fusion modifies phenotypes of microglia in neuroinflammation. *Scientific Reports*, 7(1), 4942. <https://doi.org/10.1038/s41598-017-05232-0>
- Kelly, B., & O'Neill, L. A. J. (2015). Metabolic reprogramming in macrophages and dendritic cells in innate immunity. *Cell Research*, 25(7), 771–784. <https://doi.org/10.1038/cr.2015.68>
- Khacho, M., Tarabay, M., Patten, D., Khacho, P., MacLaurin, J. G., Guadagno, J., ... Slack, R. S. (2014). Acidosis overrides oxygen deprivation to maintain mitochondrial function and cell survival. *Nature Communications*, 5, 3550. <https://doi.org/10.1038/ncomms4550>
- Kim, H., Lee, J. Y., Park, K. J., Kim, W.-H., & Roh, G. S. (2016). A mitochondrial division inhibitor, Mdivi-1, inhibits mitochondrial fragmentation and attenuates kainic acid-induced hippocampal cell death. *BMC Neuroscience*, 17, 33. <https://doi.org/10.1186/s12868-016-0270-y>
- Koning, G., Leverin, A. L., Nair, S., Schwendemann, L., Ek, J., Carlsson, Y., ... Hagberg, H. (2017). Magnesium induces preconditioning of the neonatal brain via profound mitochondrial protection. *Journal of Cerebral Blood Flow & Metabolism*. <https://doi.org/10.1177/0271678x17746132>
- Krauss, S., Zhang, C.-Y., & Lowell, B. B. (2005). The mitochondrial uncoupling-protein homologues. *Nature Reviews Molecular Cell Biology*, 6, 248–261. <https://doi.org/10.1038/nrm1592>
- Krawczyk, C. M., Holowka, T., Sun, J., Blagih, J., Amiel, E., DeBerardinis, R. J., ... Pearce, E. J. (2010). Toll-like receptor-induced changes in glycolytic metabolism regulate dendritic cell activation. *Blood*, 115(23), 4742–4749. <https://doi.org/10.1182/blood-2009-10-249540>
- Krishnan, M. L., Van Steenwinkel, J., Schang, A. L., Yan, J., Arnadottir, J., Le Charpentier, T., ... Gressens, P. (2017). Integrative genomics of microglia implicates DLG4 (PSD95) in the white matter development of preterm infants. *Nature Communications*, 8(1), 428. <https://doi.org/10.1038/s41467-017-00422-w>
- Leaw, B., Nair, S., Lim, R., Thornton, C., Mallard, C., & Hagberg, H. (2017). Mitochondria, bioenergetics and excitotoxicity: New therapeutic targets in perinatal brain injury. *Frontiers in Cellular Neuroscience*, 11(199). <https://doi.org/10.3389/fncel.2017.00199>
- Lu, Y.-T., Li, L.-Z., Yang, Y.-L., Yin, X., Liu, Q., Zhang, L., ... Qi, L.-W. (2018). Succinate induces aberrant mitochondrial fission in cardiomyocytes through GPR91 signaling. *Cell Death & Disease*, 9(6), 672. <https://doi.org/10.1038/s41419-018-0708-5>
- Mills, E. L., Kelly, B., Logan, A., Costa, A. S., Varma, M., Bryant, C. E., ... O'Neill, L. A. (2016). Succinate dehydrogenase supports metabolic repurposing of mitochondria to drive inflammatory macrophages. *Cell*, 167(2), 457–470. <https://doi.org/10.1016/j.cell.2016.08.064>
- Moss, D. W., & Bates, T. E. (2001). Activation of murine microglial cell lines by lipopolysaccharide and interferon-gamma causes NO-mediated decreases in mitochondrial and cellular function. *The European Journal of Neuroscience*, 13(3), 529–538.
- Mottahedin, A., Svedin, P., Nair, S., Mohn, C. J., Wang, X., Hagberg, H., ... Mallard, C. (2017). Systemic activation of Toll-like receptor 2 suppresses mitochondrial respiration and exacerbates hypoxic-ischemic injury in the developing brain. *Journal of Cerebral Blood Flow and Metabolism*, 37, 1192–1198. <https://doi.org/10.1177/0271678x17691292>
- Nasrallah, C. M., & Horvath, T. L. (2014). Mitochondrial dynamics in the central regulation of metabolism. *Nature Reviews Endocrinology*, 10(11), 650–658. <https://doi.org/10.1038/nrendo.2014.160>
- Niatsetskeya, Z. V., Sosunov, S. A., Matsiukevich, D., Utkina-Sosunova, I. V., Ratner, V. I., Starkov, A. A., & Ten, V. S. (2012). The oxygen free radicals originating from mitochondrial complex I contribute to oxidative brain injury following hypoxia-ischemia in neonatal mice. *The Journal of Neuroscience*, 32(9), 3235–3244. <https://doi.org/10.1523/jneurosci.6303-11.2012>
- Orihuela, R., McPherson, C. A., & Harry, G. J. (2016). Microglial M1/M2 polarization and metabolic states. *British Journal of Pharmacology*, 173(4), 649–665. <https://doi.org/10.1111/bph.13139>
- Park, J., Choi, H., Min, J. S., Park, S. J., Kim, J. H., Park, H. J., ... Lee, D. S. (2013). Mitochondrial dynamics modulate the expression of pro-inflammatory mediators in microglial cells. *Journal of Neurochemistry*, 127(2), 221–232. <https://doi.org/10.1111/jnc.12361>
- Park, J., Min, J. S., Kim, B., Chae, U. B., Yun, J. W., Choi, M. S., ... Lee, D. S. (2015). Mitochondrial ROS govern the LPS-induced pro-inflammatory response in microglia cells by regulating MAPK and NF-kappaB pathways. *Neuroscience Letters*, 584, 191–196. <https://doi.org/10.1016/j.neulet.2014.10.016>
- Park, J., Choi, H., Kim, B., Chae, U., Lee, D. G., Lee, S. R., ... Lee, D. S. (2016). Peroxiredoxin 5 (Prx5) decreases LPS-induced microglial activation through regulation of Ca(2+)/calcineurin-Drp1-dependent mitochondrial fission. *Free Radical Biology & Medicine*, 99, 392–404. <https://doi.org/10.1016/j.freeradbiomed.2016.08.030>
- Peacock, J. L., Marston, L., Marlow, N., Calvert, S. A., & Greenough, A. (2012). Neonatal and infant outcome in boys and girls born very prematurely. *Pediatric Research*, 71(3), 305–310. <https://doi.org/10.1038/pr.2011.50>
- Peiris-Pagès, M., Bonuccelli, G., Sotgia, F., & Lisanti, M. P. (2018). Mitochondrial fission as a driver of stemness in tumor cells: mDIV1 inhibits mitochondrial function, cell migration and cancer stem cell (CSC) signalling. *Oncotarget*, 9(17), 13254–13275. <https://doi.org/10.18632/oncotarget.24285>
- Pickles, S., Vigie, P., & Youle, R. J. (2018). Mitophagy and quality control mechanisms in mitochondrial maintenance. *Current Biology*, 28(4), R170–r185. <https://doi.org/10.1016/j.cub.2018.01.004>
- Raju, T. N. K., Buist, A. S., Blaisdell, C. J., Moxey-Mims, M., & Saigal, S. (2017). Adults born preterm: A review of general health and system-specific outcomes. *Acta Paediatrica*, 106, 1409–1437. <https://doi.org/10.1111/apa.13880>
- Ruiz, A., Alberdi, E., & Matute, C. (2018). Mitochondrial division inhibitor 1 (mdivi-1) protects neurons against excitotoxicity through the modulation of mitochondrial function and intracellular Ca(2+) signaling. *Frontiers in Molecular Neuroscience*, 11, 3. <https://doi.org/10.3389/fnmol.2018.00003>
- Schang, A.-L., Van Steenwinkel, J., Chevenne, D., Alkmark, M., Hagberg, H., Gressens, P., & Fleiss, B. (2014). Failure of thyroid hormone treatment to prevent inflammation-induced white matter injury in the immature brain. *Brain, Behavior, and Immunity*, 37(100), 95–102. <https://doi.org/10.1016/j.bbi.2013.11.005>
- Schuster, S., Boley, D., Moller, P., Stark, H., & Kaleta, C. (2015). Mathematical models for explaining the Warburg effect: A review focussed on ATP and biomass production. *Biochemical Society Transactions*, 43(6), 1187–1194. <https://doi.org/10.1042/bst20150153>
- Shim, S. H., Xia, C., Zhong, G., Babcock, H. P., Vaughan, J. C., Huang, B., ... Zhuang, X. (2012). Super-resolution fluorescence imaging of organelles in live cells with photoswitchable membrane probes. *Proceedings of the National Academy of Sciences of the United States of America*, 109(35), 13978–13983. <https://doi.org/10.1073/pnas.1201882109>
- Shiow, L. R., Favrais, G., Schirmer, L., Schang, A. L., Cipriani, S., Andres, C., ... Rowitch, D. H. (2017). Reactive astrocyte COX2-PGE2 production inhibits oligodendrocyte maturation in neonatal white matter injury. *Glia*, 65(12), 2024–2037. <https://doi.org/10.1002/glia.23212>
- Shitara, H., Kaneda, H., Sato, A., Iwasaki, K., Hayashi, J., Taya, C., & Yonekawa, H. (2001). Non-invasive visualization of sperm mitochondria behavior in transgenic mice with introduced green fluorescent protein (GFP). *FEBS Letters*, 500(1–2), 7–11.
- So, E. C., Hsing, C. H., Liang, C. H., & Wu, S. N. (2012). The actions of mdivi-1, an inhibitor of mitochondrial fission, on rapidly activating delayed-rectifier K(+) current and membrane potential in HL-1 murine atrial cardiomyocytes. *European Journal of Pharmacology*, 683(1–3), 1–9. <https://doi.org/10.1016/j.ejphar.2012.02.012>
- Solito, E., & Sastre, M. (2012). Microglia function in Alzheimer's disease. *Frontiers in Pharmacology*, 3, 14. <https://doi.org/10.3389/fphar.2012.00014>
- Song, Z., Ghochani, M., McCaffery, J. M., Frey, T. G., & Chan, D. C. (2009). Mitofusins and OPA1 mediate sequential steps in mitochondrial



- membrane fusion. *Molecular Biology of the Cell*, 20(15), 3525–3532. <https://doi.org/10.1091/mbc.E09-03-0252>
- Van Steenwinckel, J., Schang, A. L., Krishnan, M. L., Degos, V., Delahaye-Duriez, A., Bokobza, C., . . . Gressens, P. (2018). Loss of the Wnt/ β -catenin pathway in microglia of the developing brain drives pro-inflammatory activation leading to white matter injury. *Biorxiv Preprint* doi:<https://doi.org/10.1101/334359>
- Tay, T. L., Savage, J. C., Hui, C. W., Bisht, K., & Tremblay, M. E. (2017). Microglia across the lifespan: From origin to function in brain development, plasticity and cognition. *The Journal of Physiology*, 595(6), 1929–1945. <https://doi.org/10.1113/JP272134>
- Thion, M. S., Low, D., Silvin, A., Chen, J., Grisel, P., Schulte-Schrepping, J., . . . Garel, S. (2018). Microbiome influences prenatal and adult microglia in a sex-specific manner. *Cell*, 172(3), 500–516.e516. <https://doi.org/10.1016/j.cell.2017.11.042>
- Voloboueva, L. A., Emery, J. F., Sun, X., & Giffard, R. G. (2013). Inflammatory response of microglial BV-2 cells includes a glycolytic shift and is modulated by mitochondrial glucose-regulated protein 75/mortalin. *FEBS Letters*, 587(6), 756–762. <https://doi.org/10.1016/j.febslet.2013.01.067>
- Wai, T., & Langer, T. (2016). Mitochondrial dynamics and metabolic regulation. *Trends in Endocrinology & Metabolism*, 27(2), 105–117. <https://doi.org/10.1016/j.tem.2015.12.001>
- Westermann, B. (2012). Bioenergetic role of mitochondrial fusion and fission. *Biochimica et Biophysica Acta*, 1817(10), 1833–1838. <https://doi.org/10.1016/j.bbabi.2012.02.033>
- Williams, N. C., & O'Neill, L. A. J. (2018). A role for the Krebs cycle intermediate citrate in metabolic reprogramming in innate immunity and inflammation. *Frontiers in Immunology*, 9(141). <https://doi.org/10.3389/fimmu.2018.00141>
- Wlodarczyk, A., Holtman, I. R., Krueger, M., Yogev, N., Bruttger, J., Khorooshi, R., . . . Owens, T. (2017). A novel microglial subset plays a key role in myelinogenesis in developing brain. *EMBO Journal*, 36, 3292–3308. <https://doi.org/10.15252/embj.201696056>
- Wu, M., Neilson, A., Swift, A. L., Moran, R., Tamagnine, J., Parslow, D., . . . Ferrick, D. A. (2007). Multiparameter metabolic analysis reveals a close link between attenuated mitochondrial bioenergetic function and enhanced glycolysis dependency in human tumor cells. *American Journal of Physiology. Cell Physiology*, 292(1), C125–C136. <https://doi.org/10.1152/ajpcell.00247.2006>
- Xie, N., Wang, C., Lian, Y., Zhang, H., Wu, C., & Zhang, Q. (2013). A selective inhibitor of Drp1, mdivi-1, protects against cell death of hippocampal neurons in pilocarpine-induced seizures in rats. *Neuroscience Letters*, 545, 64–68. <https://doi.org/10.1016/j.neulet.2013.04.026>
- Youle, R. J., & van der Bliek, A. M. (2012). Mitochondrial fission, fusion, and stress. *Science*, 337(6098), 1062–1065. <https://doi.org/10.1126/science.1219855>
- Zhang, Y., Liao, S., Yang, M., Liang, X., Poon, M. W., Wong, C. Y., . . . Lian, Q. (2012). Improved cell survival and paracrine capacity of human embryonic stem cell-derived mesenchymal stem cells promote therapeutic potential for pulmonary arterial hypertension. *Cell Transplantation*, 21(10), 2225–2239. doi:<https://doi.org/10.3727/096368912x653020>
- Zhang, B., Davidson, M. M., Zhou, H., Wang, C., Walker, W. F., & Hei, T. K. (2013). Cytoplasmic irradiation results in mitochondrial dysfunction and DRP1-dependent mitochondrial fission. *Cancer Research*, 73(22), 6700–6710. <https://doi.org/10.1158/0008-5472.can-13-1411>

SUPPORTING INFORMATION

Additional supporting information may be found online in the Supporting Information section at the end of the article.

How to cite this article: Nair S, Sobotka KS, Joshi P, et al. Lipopolysaccharide-induced alteration of mitochondrial morphology induces a metabolic shift in microglia modulating the inflammatory response in vitro and in vivo. *Glia*. 2019;1–15. <https://doi.org/10.1002/glia.23587>